ANALYSES OF CORE SKEWING INFLUENCE IN PERMANENT MAGNET SYNCHRONOUS MACHINE BY 2D FEM FIELD COMPUTATION

L. MELCESCU, M. COVRIG, A. MORARU*

În articol se prezintă analiza numerică, prin metoda elementelor finite, a câmpului magnetic dintr-o secțiune transversală a unei maşini sincrone cu magneți permanenți (MSMP). În cazul acestor maşini forțele de atracție dintre magneții permanenți de pe o armătură şi dinții celeilalte armături determină apariția cuplului de prindere magnetică şi oscilații suplimentare ale cuplului total. Înclinarea crestăturilor reprezintă cea mai utilizată soluție constructivă de reducere a acestui efect. În articol se prezintă metodologia de calcul a cuplului electromagnetic şi a fluxurilor fazelor, cu luarea în considerare a înclinării crestăturilor, prin prelucrarea soluțiilor unor probleme bidimensionale rezolvate pentru diferite poziții succesive ale rotorului.

The present paper discusses the numerical analysis of the magnetic field in a cross-section of a permanent magnet synchronous machine (PMSM), achieved through the finite elements method. In the case of such machines, the attraction forces, developed between the permanent magnets on an armature and the teeth of the other armature, generate cogging torque and torque ripple. The most commonly used manufacture alternative that diminishes this effect is the skewed lamination made core. The paper presents the computing method for the electromagnetic torque and the flux phases, taking into account the skewed core, by processing the solutions of 2D problems, solved for various successive rotor positions.

Keywords: 2D finite elements method (2D-FEM), permanent magnet (PM), permanent magnet synchronous machines (PMSM), cogging torque.

Introduction

The progress achieved in permanent magnet manufacturing, together with the one obtained in power electronics, by means of integrating the semiconductor devices with DSP computing systems, resulted in an increased use of permanent magnet synchronous machines, PMSM. These machines have a high power density and increased energetic performances, as compared to the asynchronous machines.

The presence of permanent magnets on one of the armatures generates attraction forces between them and the teeth of the other armature and produces

* Lect., Prof., Dept. of Electrical Machines, Materials and Drives, Prof., Dept. of Theoretical Electrotechnics, University POLITEHNICA of Bucharest, Romania

the cogging torque, which will demand that the rotor should be aligned in certain positions in the absence of currents, and cause supplementary torque ripple on load condition.

In general, the PMSM ripple torque is induced by the harmonics of the normal component of the air-gap flux density curve and the winding currents harmonics. These produce vibrations and noises, which can increase at variable speeds, when the frequency of the ripple torque coincides with the various frequencies of the mechanical components of the machines [3].

Adapting drive current waveforms can diminish torque ripple, but high performance is obtained by means of optimizing the air-gap flux density space distribution.

To this purpose, many construction solutions are employed: slot skewing, slot width reduction, magnet burial into the rotor core, magnetic poles magnetization variation [4], bifurcated teeth, asymmetrical placed by half tooth positioning of the poles represented by the magnets [5], use of fractional slot/pole, or direct placing of the winding in the air-gap in the slotless machine case [6].

The most frequently used method consists in slot skewing by a tooth pitch [7]. Most precise computing methods are required for analysing and minimising the ripple torque as early as the designing stage.

Finite element numerical analysis is one of the modern methods used in electrical machines design. The instantaneous torque value can be accurately computed starting from the numerical solution of the field problem.

1. FEM Analyses of Electromagnetic Field

The electromagnetic field was computed for a three phase permanent magnet synchronous machine, made by ICPE-SERVOMOTORS, with the following rates: $P_N = 4$kW, $M_N = 9.6$Nm, $I_N = 9.3$A, $M_{0m} = 16$Nm, $I_{0m} = 14.9$A, $k_E = =65$V/krpm, $K_T = 1.075$Nm/A. The permanent magnets are placed in the air-gap and the machine has six poles. The numerical field problem was solved by FEM in MATLAB environment using the PDE Toolbox function.

The mesh grid of the computation domain represented by a cross section is shown in Fig. 1. In order to ensure a relative movement between the rotor and the stator, a slipping line was placed in the middle of the air-gap, uniformly divided into equal arcs. Here, the movement of the rotor by a minimum $\Delta\theta = 5°$ step is allowed.

For a given rotor position and an instant time, the electromagnetic field structure in the PM synchronous machine is of magnetostatic type. The field equation corresponding in the cross-section, Fig. 1, is

$$\operatorname{curl}\left[\boldsymbol{\nu}(\mathbf{B})\cdot\operatorname{curl}\mathbf{A}\right] = \mathbf{J} + \operatorname{curl}\left[\left(\boldsymbol{\nu}(\mathbf{B})/\boldsymbol{\nu}_0\right)\cdot\mathbf{M}_p\right] \tag{1}$$

where $\mathbf{A}$ is the magnetic potential vector, $\boldsymbol{\nu}$ is the reluctivity of the material,

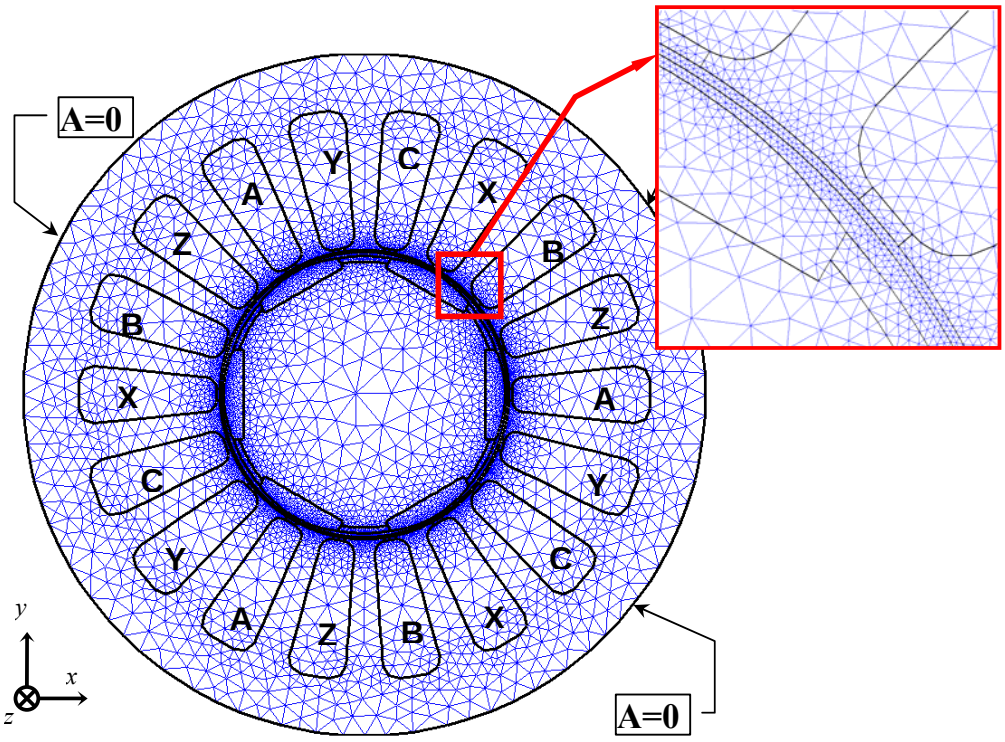

Fig. 1. Mesh grid of computation domain and boundary conditions

J the stator current density and $\mathbf{M}_p$ the magnetization of the permanent magnets. In the chosen computation domain, the magnetic potential vector and the current density have only the axial component on the *z*-axis, and the flux density and magnetization have components only on the *x* and *y* axes.

By linearising the demagnetisation characteristic of the NdFeB magnet, fig 2.a, a relative permeability, μ_{rmag}=1.0362, is obtained, in the regions in which they are placed. The contribution of the magnets to the total field is taken into account by means of some superficial currents on their border. Due to the radial magnetisation direction of the magnets, the equivalent currents have an axial component exclusively.

The reluctivity of the slot and air-gap regions is equal to the vacuum reluctivity: $\nu_0=10^7/(4\pi)$ (m/H). The B(H) dependence in the core regions, Fig. 2.b, leads to a nonlinear problem.

For finding the values of the magnetic vector potential in the mesh grid nodes, the boundary conditions must be added to the above equation (1). These are of homogenous Dirichlet type, **A**=0.

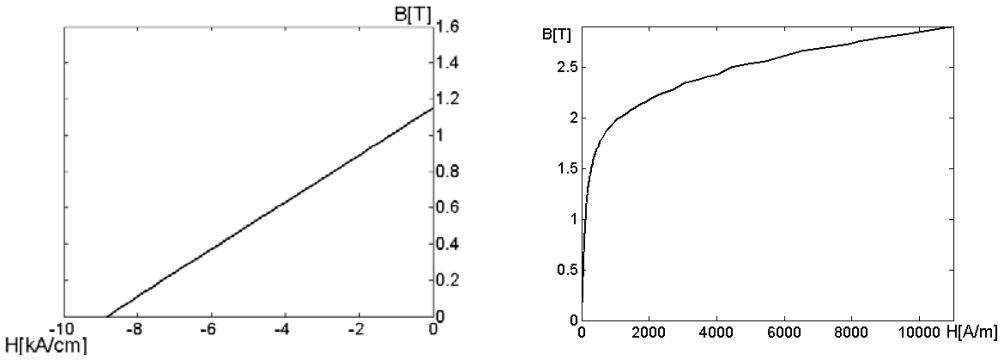

(a) (b)

Fig.2. Material characteristic: (a) demagnetisation curve of NdFeB permanent magnets. (b) magnetisation curve of magnetic core.

In Matlab-PDE Toolbox environment, the magnetic potential has a linear variation, [11] in each *e* element, Fig.3:

$$A^e(x,y)=\sum_{k=1}^{3}\frac{1}{2\Delta^e}\left(a^e_{P_k}+b^e_{P_k}x+c^e_{P_k}y\right)A^e_{P_k}\ . \tag{2}$$

where a^e_{Pk}, b^e_{Pk}, c^e_{Pk} were computed based on the coordinates of the P_1, P_2 and P_3 nodes:

$$\begin{vmatrix} a^e_{P_1} & b^e_{P_1} & c^e_{P_1} \\ a^e_{P_2} & b^e_{P_2} & c^e_{P_2} \\ a^e_{P_3} & b^e_{P_3} & c^e_{P_3} \end{vmatrix} = \begin{vmatrix} x_{P_2}y_{P_3}-x_{P_3}y_{P_2} & y_{P_2}-y_{P_3} & x_{P_3}-x_{P_2} \\ x_{P_3}y_{P_1}-x_{P_1}y_{P_3} & y_{P_3}-y_{P_1} & x_{P_1}-x_{P_3} \\ x_{P_1}y_{P_2}-x_{P_2}y_{P_1} & y_{P_1}-y_{P_2} & x_{P_2}-x_{P_1} \end{vmatrix}. \tag{3}$$

In (2), Δ^e represents the area of the *e* element, which is computed by:

$$\Delta^e=\frac{1}{2}\left(b^e_{P_1}c^e_{P_2}+b^e_{P_1}c^e_{P_2}\right) \tag{4}$$

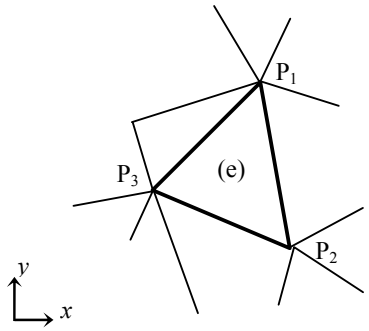

Fig.3. The used *e* element notation

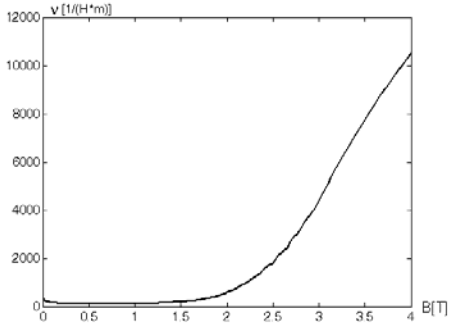

Fig.4. ν/B dependences

The PDE Toolbox functions provide the equation system [K]{*A*}={*b*}, according to equation (1), with the above mentioned boundary conditions. On the source current density vector {*b*}, the contribution of the equivalent superficial currents must be added for the nodes on the magnet borders, [2]. If the P_1 and P_2 nodes of the *e* triangular element, Fig.3., have the *i* and *j* notation in the global notations, the matrix [K] elements have the following expression:

$$K_{ij} = \sum_{e}^{m_i} \left[\frac{\nu^e}{4\Delta^e} \left(b^e_{P_1} b^e_{P_2} + c^e_{P_1} c^e_{P_2} \right) \right]. \tag{5}$$

The obtained equation system is of nonlinear type due to the fact that the elements of matrix [K] depend on the system solution. Solving is made by the use of Newton-Raphson method, accelerated by the use of a subrelaxation coefficient found by the optimal method, [2]. The initialization is made by solving a linear problem, in which the relative permeability of magnetic core regions is μ_{rFE}=500.

On each iteration step, the equation system is solved by the conjugated

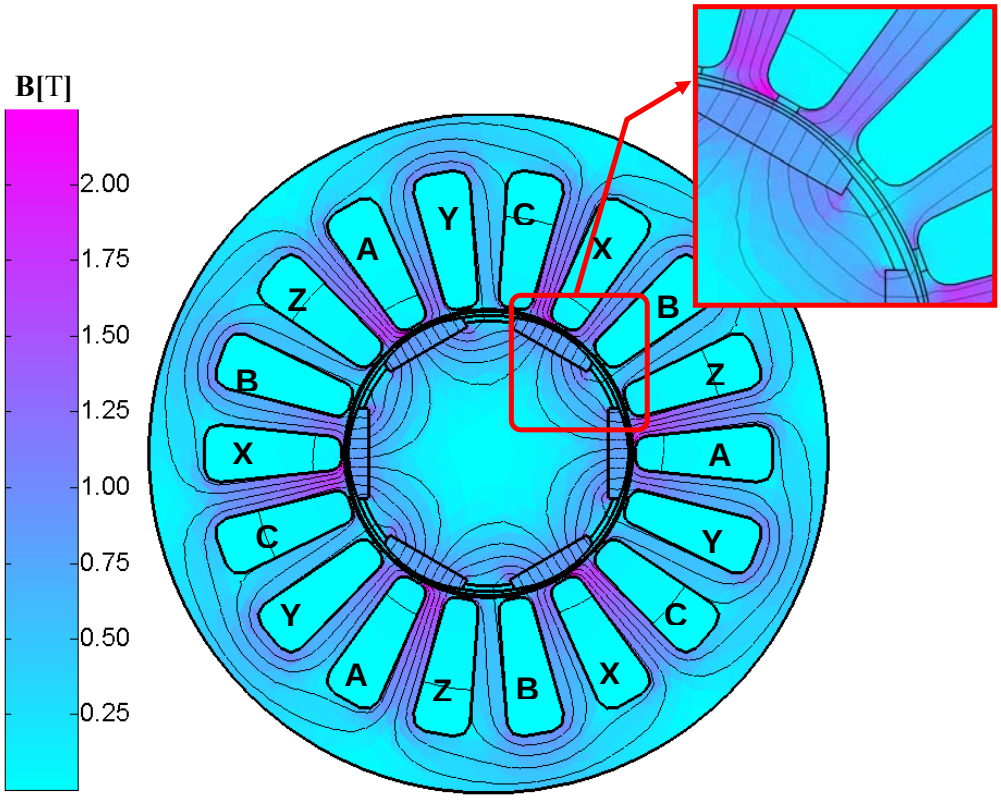

Fig.5. Flux density chart and equi-flux lines

gradient method [2]. The new values for the reluctivity of the magnetic core elements are found out from the ν=ν(B) curve, Fig.4., by spline interpolation of flux density module values, computed through relation (6):

$$B^e = \sqrt{\left(B_x^e\right)^2 + \left(B_y^e\right)^2} = \sqrt{\left(\frac{\partial A^e}{\partial y}\right)^2 + \left(-\frac{\partial A^e}{\partial x}\right)^2} = \\ = \sqrt{\left(\frac{1}{2\Delta^e}\sum_{k=1}^{3} c_{P_k}^e A_{P_k}^e\right)^2 + \left(-\frac{1}{2\Delta^e}\sum_{k=1}^{3} b_{P_k}^e A_{p_k}^e\right)^2} \tag{6}$$

The iterative procedure continues until the relative increment of the solution becomes less than the imposed precision:

$$\varepsilon^k = \frac{\left\|\Delta\{A\}^k\right\|}{\left\|\{A\}^k\right\|} < \varepsilon_{imposed}, \tag{7}$$

where $\|\{A\}\|$ is the Euclidian norm of node solution vector.

The flux density chart and the equi-flux lines are shown in Fig.5 for a sinusoidal load current with an I_{max}=14 A amplitude value. The currents phases were chosen so that the field axes of the stator and the rotor should be orthogonal. In order to comply with this requirement, phase *A* current must have the maximum value for the rotor position in Fig.1. The current density values in the slots were computed by relation (8) for ωt=π/2:

$$\begin{cases} J_A = -J_X = I\sqrt{2}\,\dfrac{N_{sp}}{S_c}\sin(\omega t) \\ J_B = -J_Y = I\sqrt{2}\,\dfrac{N_{sp}}{S_c}\sin\left(\omega t - \dfrac{2\pi}{3}\right) \\ J_C = -J_Z = I\sqrt{2}\,\dfrac{N_{sp}}{S_c}\sin\left(\omega t - \dfrac{4\pi}{3}\right) \end{cases} . \tag{8}$$

In the above relations, N_{sp} is the number of the slot turns, and S_c is the slot area.

2. Torque Computation

The electromagnetic torque values can be found from the field problem solution. Two methods are used for the rotating machines with saliency: Maxwell's stress tensor method and the virtual work method.

The first one consists in the integration of Maxwell's stress tensor on the closed surface around the moving body [1]. In the case of 2D problems, the integral is transformed in the sum of the products between the normal components

of the flux density and the tangential components of the magnetic force on the chosen path. This method may be affected by errors because the magnetic vector potential formulation does not ensure the continuity of the tangential component of the magnetic field intensity on the element borders.

The virtual work method ensures more accuracy in torque computation and is more attractive for electrical machine designers, [9]. The electromagnetic torque of rotating machines can be computed by applying the generalized forces theorem:

$$M = -\frac{\partial W_m}{\partial \theta}\bigg|_{\Psi=const.}, \tag{9}$$

where W_m is the magnetic energy, θ the generalised coordinate and Ψ the magnetic flux.

Using the jacobian matrix with the local derivatives, Coulomb [9], and Coulomb and Meunier [10], replaced relation (9) with:

$$M = -\frac{\partial W_m}{\partial \theta}\bigg|_{\Psi=const.} = -\frac{1}{2} L \{A\}^t \left[\frac{\partial \mathrm{K}}{\partial \theta}\right] \{A\}, \tag{10}$$

where [K] is the FEM matrix, $\{A\}$ is the node magnetic potential vector, and L the ideal machine length.

The derivatives of the FEM matrix elements are calculated through:

$$\frac{\partial \mathrm{K}_{ij}}{\partial \theta} = \sum_{e}^{m_i} \frac{\nu^e}{4\left(\Delta^e\right)^2} \left[\Delta^e \frac{\partial}{\partial \theta}\left(b^e_{P_1} b^e_{P_2} + c^e_{P_1} c^e_{P_2}\right) - \left(b^e_{P_1} b^e_{P_2} + c^e_{P_1} c^e_{P_2}\right)\frac{\partial \Delta^e}{\partial \theta}\right]. \tag{11}$$

For a rotating movement around the Oz axis, that intersects the xOy plane in a point having the (a,b) coordinates, the derivatives of the node coordinates, with respect to the virtual displacement, are [4]:

$$\frac{\partial x_i}{\partial \theta} = -p_i y_i + b \qquad \frac{\partial y_i}{\partial \theta} = p_i x_i - a\,. \tag{12}$$

The values of the p_i coefficients belong to the [0,1] interval. The p_i values are 1 for the nodes placed in the rotor regions and for the rotor surface nodes that have the same virtual displacement. The p_i values are 0 for the nodes placed in the stator regions and for the stator surface nodes that are fixed. For the air-gap nodes the p_i coefficients have arbitrary values between 0 and 1.

3. Flux Computation

The total coil flux is computed as the sum of circulation of potential magnetic vector along each path, Γ, which goes through the mass centers of the triangles in the coil regions, Fig. 4:

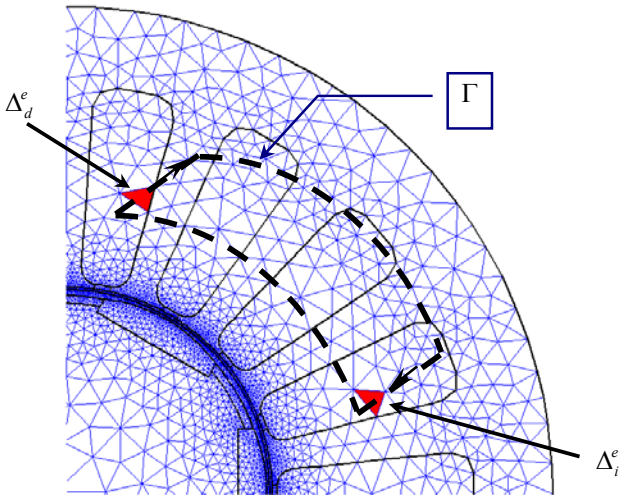

Fig.6. Integration path of magnetic potential
for phase flux computation

$$\Phi_b = L\left[\sum_{e=1}^{Nd} N_{edm} A_{dm}^e - \sum_{e=1}^{Ni} N_{eim} A_{im}^e\right]. \tag{13}$$

In the above relation, L is the ideal machine length; Nd and Ni designates the number of triangular elements of the coil regions in the slot. They correspond to the going turns, and to the return ones, respectively.

The potentials in the mass centers of the triangles, A_{im}^e and A_{dm}^e equal the averages of the potentials of the elements node:

$$A_{dm}^e = \frac{1}{3}\left(A_{dP_1}^e + A_{dP_2}^e + A_{dP_3}^e\right) \qquad A_{im}^e = \frac{1}{3}\left(A_{iP_1}^e + A_{iP_2}^e + A_{iP_3}^e\right). \tag{14}$$

The average numbers of coils in the triangular elements, noted N_{edm} and N_{eim} in (13), are computed by:

$$N_{edm} = N_b \frac{\Delta_d^e}{S_c} \qquad N_{eim} = N_b \frac{\Delta_d^i}{S_c}, \tag{15}$$

where N_b represents the number of coil turns, S_c is the slot area and Δ_d^e and Δ_i^e the areas of the regions, of the going turns, and of the return ones, respectively.

In the present case, the phase winding is obtained by the series connecting of the coils of each pair of poles. The phase flux is computed by:

$$\Phi = p\Phi_b, \tag{16}$$

where p is the number of pair poles.

4. Torque and Flux Computation in the Case Core Skewing

The numerical analysis of the skewed core slots calls for a 3D approach of the field problem. It is possible to take into account the influences of the skewed core, by processing the solutions of 2D problems, solved for various positions of the rotor, and for the same values of the winding currents.

If, for the same current values, the values of the phase fluxes and the torque are known for n successive rotor positions along a pitch pole τ_c, the skewed core, with L as axial length, will be taken into account by an equivalation of the real skewed lamination made core with n unskewed lamination made cores, with L/n axial length, which are spaced with τ_c/n, Fig. 7.

The electromagnetic torque, M_e`, and the phase fluxes, $\Psi`_k$, in the case of the skewed core can be computed by averaging the values computed through relation (10) and (13) respectively, for those n successive rotor positions:

$$M'_e(i_A,i_B,i_C,\theta)=\frac{1}{n}\sum_{p=0}^{n}M_e\left(i_A,i_B,i_C,\theta+\frac{\tau_c}{n}p\right)$$
$$\Psi'_k(i_A,i_B,i_C,\theta)=\frac{1}{n}\sum_{p=0}^{n}\Psi_k\left(i_A,i_B,i_C,\theta+\frac{\tau_c}{n}p\right),\qquad k=A,B,C \tag{17}$$

The cogging torque variation with rotor position in the cases of both skewed and unskewed cores is comparatively shown in Fig.8. The cogging torque is null for the pole axis coinciding with the tooth or slot axis, and for other two intermediate positions. In the absence of stator currents, the rotor positions itself in the places of maximum torque. It can be observed that skewing the teeth by one tooth pitch will lead to a significant reduction, by approximately 90%, of the cogging torque peak value.

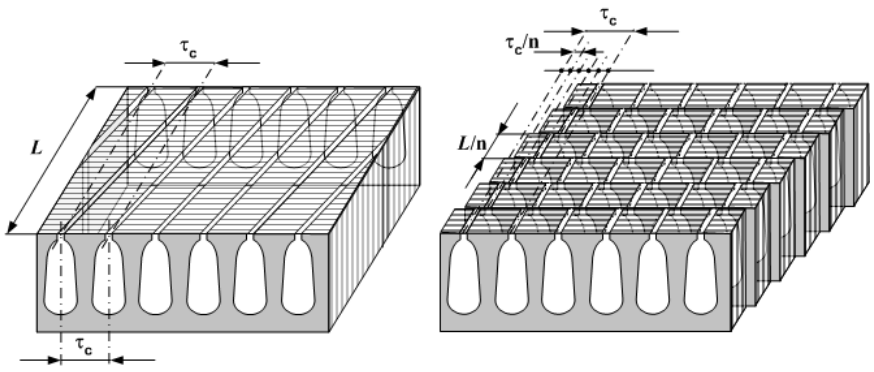

Fig.7. Equivalence of the real skewed core with some more spaced unskewed cores.

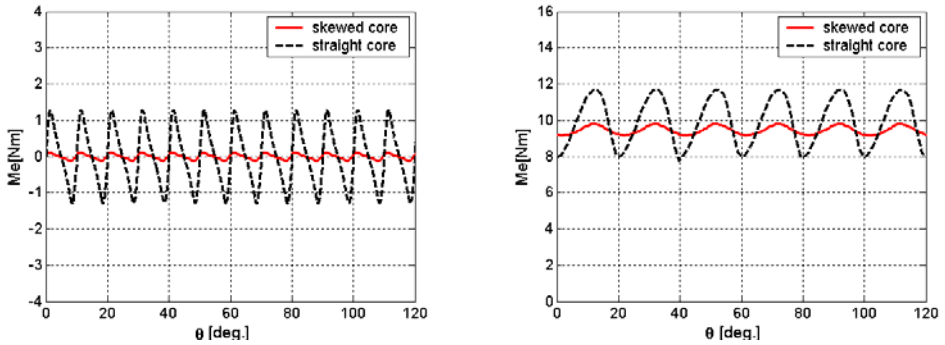

(a) (b)

Fig. 8. The effects of skewed stator core on the torque variation:
(a) cogging torque, (b) ripple of torque at rated load

The torque variation with the rotor position in the rated load regime is presented in Fig. 8.b. The stator currents have the rated values and the field they produce is perpendicular on the rotor field. It can be noted that the number of ripple pulses equals the number of the slots. Skewing the teeth by one tooth pitch will produce a decrease of the ripple torque peak value, by approximately 85%, and a small reduction of medium torque value from 9.85 Nm to 9.5 Nm.

In the case of the skewed core, the waveform of a phase flux has a diminished content of harmonics, Fig. 9.a. In the case of the unskewed core, it is slightly flattened, due to the magnetic core saturation.

During experimental trials, due to the lack of access to the common point of the star connection, only the phase-to phase voltages and currents were measured. The time depending evolution of phase-to-phase voltages was recorded in no-load generator regime.

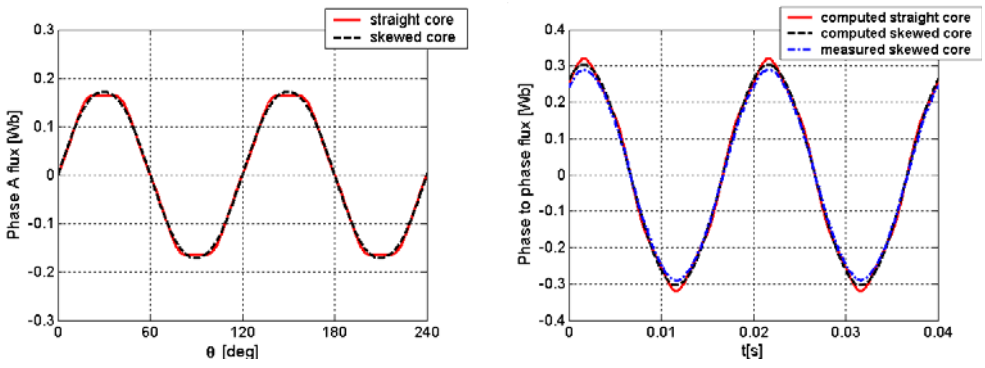

(a) (b)

Fig. 9. Influence of stator core skew of flux variation in no load condition:
(a) Phase flux versus rotor position. (b) Phase to phase flux time dependence.

Table 1

Harmonic analyses of flux variation

			$\Psi_{[mWb]}$ RMS	Harmonic Amplitude							THD [%]
					Harmonic order							
					1	3	5	7	9	11	13	
Phase flux	Computed	Straight core	125.00	[mWb]	176.50	4.96	7.26	0.49	0.16	0.69	0.12	**5.01**
				[%]	100.00	2.81	4.11	0.28	0.09	0.39	0.07	
		Skewed core	123.70	[mWb]	174.90	2.97	0.69	0.10	0.03	0.01	0.02	**1.75**
				[%]	100.00	1.70	039	0.03	0.02	0.00	0.01	
Phase to phase flux	Computed	Straight core	216.40	[mWb]	305.70	0.00	12.57	0.85	0.00	1.21	0.20	**4.14**
				[%]	100.00	0.00	4.11	0.28	0.00	0.39	0.07	
		Skewed core	214.20	[mWb]	302.90	0.00	1.19	0.17	0.00	0.01	0.03	**0.40**
				[%]	100.00	0.00	0.39	0.06	0.00	0.00	0.01	
	Measured	Skewed core	203.50	[mWb]	287.70	0.00	2.53	0.07	0.00	0.12	0.04	**1.31**
				[%]	100.00	0.00	0.88	0.02	0.00	0.04	0.02	

The time depending evolution of the difference between the fluxes of two phases (phase-to-phase flux) was computed by numerical integration. Fig. 9.b. shows a comparison between the measured values and the calculated ones in skewed and unskewed core cases, in no-load generator regime, at 1000 rpm.

Table 1 shows the harmonic analyses and the total harmonic distortions, THD, of the waveforms in Fig. 9. It can be noted that the skewed lamination made core leads to a significant reduction of the 5th harmonic from the phase flux curve and to a smaller reduction of 3rd harmonic, whose influence is annulled by the star connection.

The differences between the measured values and the calculated ones mainly come from the magnetisation curve that was used, Fig. 2.b., which is not identical with the real one of the core.

Conclusions

The paper presents the numerical computation methodology for the phase fluxes and for the electromagnetic torque of a PMSM, taking into consideration the magnetic core non-linearity and the skewed lamination made core.

Even if the analysis of the skewed core slots calls for a 3D approach, the proposed algorithm use the 2D numerical modelling of the magnetic field in magnetostatic regime, through the finite element method.

The modelling of the slots skewed is performed through an equivalation of the real skewed lamination made core with some more unskewed lamination made cores, which are spaced. The number of these equivalent cores equals the number of the successive rotor positions in the interval matching the skewing size. The phase fluxes and the torque are computed by averaging the results of the problems solved for these successive rotor positions, and for the same values of the winding currents.

By applying this computation method, it becomes obvious, even from the designing stage, that the advantages obtained by ripple torque reduction compensate the flux and the average torque decrease as a result of tooth skew, and justify the use of a more complex manufacturing technology.

REFERENCES

1. *C. Mocanu*, Bazele Electrotehnicii - Teoria câmpului electromagnetic, Editura Didactică şi pedagogică Bucureşti – 1991.
2. *L. Melcescu*, Modele Matematice Pentru Reprezentarea Magneților Permanenți, Referat teza doctorat, Universitatea Politehnica Bucureşti, Catedra Electrotehnica, 2001.
3. *D. Howe and Z.Q. Zhu*, The Influence of Finite Element Discretisation on the Prediction of Cogging Torque in Permanent Magnet Excited Motors, IEEE Trans. Magn., **Vol. 28**, N0.2, 1992, pp. 1080-1083;
4. *R P. Deodhar, D. A. Staton, T. M. Jahns, T. J. E. Miller*; Prediction of Cogging Torque Using the Flux-MMF Diagram Technique, IEEE Trans. Ind. Applicat., **Vol. 32**, N0.3, 1996, pp. 569-576;
5. *P. Minciunescu*, Boundary Element Method in Reduction of Cogging Torque, IEEE Trans. Magn., **Vol.34**, Nr. 5, 1994, pp 2905-2907;
6. *M.Jufer*; Slotless and Slotted Brushless DC Motors. Technique Performances and Comparison, ELECTROMOTION, **Vol. 4**, N0.1-2, 1997, pp. 69-79;
7. *N. Vasile, V. Dogaru, C. Sălişteanu*; Maşini Electrice - Construcție, Tehnologie, Aplicații speciale, Editura ICPE, Bucureşti 2000;
8. *N. Vasile*, Forțele parazite în motoarele lineare sincrone cu magneți permanenți, Editura ICPE, Bucureşti 1997;
9. *J.L.Coulomb*, A methodology for the determination of global electromechanical quantities from a finite element analysis and its application to the evaluation of magnetic forces, torques and stiffness, IEEE Trans. Magn., **Vol.19**, 1983, pp 2514-2519;
10. *J.L.Coulomb and G.Meunier*, Finite element implementation of virtual work principle for magnetic or electric force and torque computation, IEEE Trans. Magn., **Vol.20**, 1984, pp 1894-1896;
11. *MATLAB*©, Partial Differential Equation Toolbox User's Guide, The MathWorks, Inc., 1995.